Appl Phys B (2008) 93: 381–388
DOI 10.1007/s00340-008-3162-8

Applied Physics B
Lasers and Optics

Optimum parameters for sideband cooling of a $^{40}Ca^{+}$ ion

H. Sawamura · K. Kanda · R. Yamazaki · K. Toyoda · S. Urabe

Received: 14 March 2008 / Revised version: 7 July 2008 / Published online: 8 September 2008

Abstract Optimum conditions for sideband cooling of $^{40}Ca^{+}$ are numerically analyzed and appropriate parameters are evaluated. The dependence of optimum parameters for sideband cooling on the realistic experimental conditions, such as laser linewidth or heating rate, is investigated. For experimental verification of the analysis, a single $^{40}Ca^{+}$ is sideband-cooled using parameters based on the analysis, and the achieved average oscillation quantum numbers are evaluated. As a result, a good agreement between the experimental value and numerical analysis is obtained.

PACS 32.80.Hd · 03.67.Lx · 37.10.Vz · 42.50.Wk

1 Introduction

As first proposed by Cirac and Zoller, a collection of ions trapped in electric potentials is currently considered as one of the probable candidates for the quantum computation [1]. One of the prerequisites for the implementation of the Cirac–Zoller proposal is that the motional mode of the ion strings used for the gate operation is prepared in its ground state. Such preparation of motional ground state can be achieved by sideband cooling. The motional ground state cooling has been theoretically analyzed [2–4], and successful demonstration of sideband cooling has been reported with $^{198}Hg^{+}$, $^{9}Be^{+}$, $^{40}Ca^{+}$, and $^{111}Cd^{+}$ [5–8]. In the theoretical analysis previously reported, however, a part of parameters that strongly affect realistic experimental situations, such as laser linewidths or heating rates, has not been thoroughly considered. Therefore, it has been difficult to extract practically valid information on the optimum values of parameters for sideband cooling to the motional ground state.

In this report, we have numerically evaluated optimum conditions for sideband cooling of three-level ions, especially $^{40}Ca^{+}$ including the effects due to the laser linewidths and heating rates. From the analysis, it is concluded that the laser linewidths and heating rates determine optimum values of other parameters such as Rabi frequencies or detunings of lasers for sideband cooling. In the recent experimental research of ion traps, operations with smaller trap have been required. Subsequently, heating rates of ion traps become higher following d^{-4} rule due to fluctuating patch potentials on the trap surfaces, where d is the distance between the ion and the closest electrode [9]. The numerical analysis introduced in this report can be utilized to investigate optimum parameters for sideband cooling even if such a high heating rate needs to be considered.

For experimental verification of the analysis, a single $^{40}Ca^{+}$ ion is sideband-cooled using parameters based on the analysis. The resulting average oscillation quantum numbers, and the optimum parameters minimizing them, are close to the values obtained from the analysis. This numerical analysis is applicable to different ion species with similar three-level structure such as Sr^{+} or Ba^{+}.

H. Sawamura (✉) · K. Kanda · K. Toyoda · S. Urabe
Graduate School of Engineering Science, Osaka University, 1-3 Machikaneyama, Toyonaka, Osaka 560-8531, Japan
e-mail: sawamura@qe.ee.es.osaka-u.ac.jp

R. Yamazaki · K. Toyoda · S. Urabe
JST-CREST, 4-1-8 Hommachi, Kawaguchi, Saitama 331-0012, Japan

2 Motional ground state cooling

2.1 Three-level system of $^{40}Ca^{+}$

Motional ground state cooling is achieved by two cooling schemes [5]. For the first step, a single ion is stored in an ion trap, and Doppler-cooled to near the Doppler limit temperature. In the case of a two-level ion, the Doppler limit is given as $T_D = \hbar\Gamma/2k_B$, where Γ denotes the spontaneous decay rate of the upper level of the cooling transition [10]. For the second step, sideband cooling is performed to cool the ion to the motional ground state.

$^{40}Ca^{+}$ is a hydrogen-like ion with one valence electron and no hyperfine structure. An energy diagram of $^{40}Ca^{+}$ relevant to the sideband cooling is shown in Fig. 1. The energy diagram forms a three-level system in Ξ-configuration. Notations $|0\rangle$, $|1\rangle$, and $|2\rangle$ represent internal states $S_{1/2}$ ($m = -1/2$), $P_{3/2}$ ($m = -3/2$), and $D_{5/2}$ ($m = -5/2$), respectively. A quadrupole transition $|0\rangle$–$|2\rangle$, whose transition wavelength is 729 nm, is used for the sideband cooling. Both $|1\rangle$–$|0\rangle$ and $|1\rangle$–$|2\rangle$ are dipole allowed transitions, and have radiative decay rates of $\Gamma_{10} = 2\pi \times 21.5$ MHz and $\Gamma_{12} = 2\pi \times 1.6$ MHz, respectively [11]. The $|2\rangle$ level has a relatively long lifetime of 1.2 s [12]. An 854 nm laser couples the $|2\rangle$ level to the $|1\rangle$ level and shortens its effective lifetime, which is called *quenching*. The quenched population decays back to the $|0\rangle$ level and the sideband cooling cycle is almost closed. By applying the 729 nm beam, which is red-detuned from a carrier transition by the motional frequency in the harmonic potentials called *secular frequency*, one vibrational quantum number is removed for each cooling cycle until attaining the motional ground state.

2.2 Principles for numerical analysis

Let us consider a three-level ion in a harmonic potential coupled with two classical laser fields. Under the assumption that the dynamics of the external motion in the harmonic potential is much slower than the internal dynamics, the internal variables can be assumed to be in a steady state, and be eliminated adiabatically. When the Lamb–Dicke parameter is non-zero, redistribution between the reduced density matrix elements for the external degree of freedom occurs. As long as the Lamb–Dicke parameter is much smaller than 1, this can be treated perturbatively, and in the steady state only diagonal elements survive. In the following, the derivation of the rate equation for the external population and the steady state is reviewed [2–4, 13, 14].

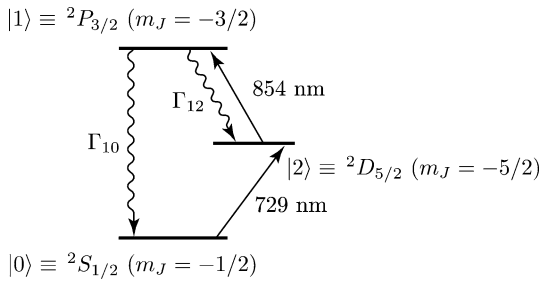

Fig. 1 Ξ-configuration three-level energy diagram relevant to the sideband cooling. Γ_{10} and Γ_{12} are decay rates between the $|1\rangle$–$|0\rangle$ and $|1\rangle$–$|2\rangle$ transitions, respectively

The master equation of the density matrix is described by

$$\frac{d\rho}{dt} = -\frac{i}{\hbar}[\mathcal{H}, \rho] - \frac{1}{2\hbar}\sum_{ij}\left(\hat{C}_{ij}^{\dagger}\hat{C}_{ij}\rho + \rho\hat{C}_{ij}^{\dagger}\hat{C}_{ij} - 2\hat{C}_{ij}\rho\hat{C}_{ij}^{\dagger}\right) \equiv \mathcal{L}\rho, \tag{1}$$

where $\mathcal{L}$ is the Liouvillian [2]. For the Ξ-configuration energy level, the Hamiltonian of the atom and atom-field interaction is given as

$$\mathcal{H} = \hbar\begin{bmatrix} 0 & 0 & \Omega_{20}/2 \\ 0 & -(\delta_{12}+\delta_{20}) & \Omega_{12}/2 \\ \Omega_{20}/2 & \Omega_{12}/2 & -\delta_{20} \end{bmatrix}, \tag{2}$$

where δ_{ij} and Ω_{ij} are the detuning and the Rabi frequency of the field coupling between $|i\rangle$ and $|j\rangle$ levels, respectively [3]. The *decay matrix* $\hat{C}_{ij}$ is given as

$$\hat{C}_{ij} = \sqrt{\Gamma_{ij}}|j\rangle\langle i|, \tag{3}$$

which represents a decay process from $|i\rangle$ to $|j\rangle$ levels. Γ_{ij} is the spontaneous decay rate between $|i\rangle$ and $|j\rangle$ levels. The linewidths of 729 and 854 nm lasers are effectively included in the terms Γ_{00} and Γ_{11}, respectively.

The cooling and heating mechanisms are considered through the evolution of the motional state population $p_n = \langle n|\rho|n\rangle$, described by the following rate equation [14]

$$\frac{dp_n}{dt} = (n+1)A_{-}p_{n+1} - \left[(n+1)A_{+} + nA_{-}\right]p_n + nA_{+}p_{n-1}. \tag{4}$$

$A_{+/-}$ is a heating/cooling transition rate given as [4]

$$A_{\pm} = 2\mathrm{Re}\left[D + S(\mp\omega)\right], \tag{5}$$

where D denotes the diffusion coefficient,

$$D = \alpha\langle\rho_{11}\rangle_{\mathrm{SS}}\left(\Gamma_{10}\eta_{10}^2 + \Gamma_{12}\eta_{12}^2\right) \tag{6}$$

due to the spontaneous emission from the excited level. The quantities with subscript SS describe the values for the steady state, and $\eta = k\sqrt{\hbar/2m\omega}\cos\theta$ is the Lamb–Dicke parameter. k, m, and ω are the wave number of the laser, the

mass of the trapped ion, and the secular frequency, respectively. θ is an angle between the laser beam and the oscillation axis. α is a constant due to the angular distribution of the spontaneous emission. It is given as $\frac{1}{10}(3+\cos^2\phi)$ for the $\sigma=\pm1$ dipole transitions [15], where ϕ is the angle between the directions of the magnetic field and the vibrational axis. In our case, α is 0.35 since the angle is $\phi=45°$. S is the power spectrum,

$$S(\omega)=\frac{1}{2m\hbar\omega}\mathrm{Tr}\big[F(-i\omega-\mathcal{L})^{-1}F\langle\rho\rangle_{\mathrm{SS}}\big] \tag{7}$$

of the dipole force,

$$F=-\frac{\hbar}{2}\Omega_{20}k_{20}\sigma_{y20}-\frac{\hbar}{2}\Omega_{12}k_{12}\sigma_{y12}, \tag{8}$$

where σ_{y20} and σ_{y12} are the y components of the Bloch vectors, which are given as

$$\sigma_{y20}=\begin{bmatrix}0&0&i\\0&0&0\\-i&0&0\end{bmatrix},\qquad \sigma_{y12}=\begin{bmatrix}0&0&0\\0&0&i\\0&-i&0\end{bmatrix}. \tag{9}$$

From (4), the time evolution of the average oscillation quantum number is given as

$$\frac{d}{dt}\langle n\rangle=-W\big(\langle n\rangle-\langle n\rangle_{\mathrm{SS}}\big), \tag{10}$$

where W is the cooling rate

$$W=A_{-}-A_{+}, \tag{11}$$

and $\langle n\rangle_{\mathrm{SS}}$ is the final oscillation quantum number

$$\langle n\rangle_{\mathrm{SS}}=\frac{A_{+}+R_{\mathrm{heat}}}{A_{-}-A_{+}}. \tag{12}$$

R_{heat} represents the heating rate, which is defined as increase of average oscillation quantum numbers per unit time in the absence of laser cooling [5].

3 Results of numerical analysis

Sideband cooling to the motional ground state is achieved by choosing the appropriate values for the parameters Ω_{20}, δ_{20}, Ω_{12}, and δ_{12}. The transition frequency between a pair of levels is shifted when 729 and 854 nm beams are applied. The shifts of the transition frequency between the pairs of $|0\rangle$ and $|2\rangle$, and $|2\rangle$ and $|1\rangle$ levels are given as

$$\begin{aligned}\tilde{\delta}_{20}&=\omega-\sqrt{\omega^2-\Omega_{20}^2},\\ \tilde{\delta}_{12}&=\frac{\Omega_{12}^2}{(\Gamma_{10}+\Gamma_{12})^2+4\delta_{12}^2}\delta_{12},\end{aligned} \tag{13}$$

respectively, in the following regimes:

$$\begin{aligned}&\omega\gg\Omega_{20},\\ &\frac{\Omega_{12}^2}{(\Gamma_{10}+\Gamma_{12})^2+4\delta_{12}^2}\ll1.\end{aligned} \tag{14}$$

δ_{20} should be adjusted to $-\omega+\tilde{\delta}_{20}+\tilde{\delta}_{12}$ to minimize $\langle n\rangle_{\mathrm{SS}}$, where δ_{20} is due to the non-resonant excitation of the carrier transition $|0\rangle$–$|2\rangle$. In this paper, we define $\langle n\rangle_{\mathrm{SS,opt}}$ as the minimized $\langle n\rangle_{\mathrm{SS}}$ by adjusting δ_{20} to the optimum value.

For the investigation of optimum values of δ_{12} and Ω_{12}, a parameter Γ_{eff}, determined by δ_{12} and Ω_{12}, is introduced. Γ_{eff} is an *effective decay rate* on the $|0\rangle$–$|2\rangle$ transition when the Ξ-configuration three-level system is regarded as an effective two-level system by eliminating the $|1\rangle$ level adiabatically. The effective decay rate of the effective two-level system is given as [3]

$$\Gamma_{\mathrm{eff}}=\frac{\Omega_{12}^2}{(\Gamma_{10}+\Gamma_{12})^2+4\delta_{12}^2}\Gamma_{10}. \tag{15}$$

$\langle n\rangle_{\mathrm{SS,opt}}$ is numerically simulated as $\eta\Omega_{20}$ is varied to evaluate the range of the optimum Γ_{eff}. The fixed parameters used for the simulation are listed in Table 1. Then the Lamb–Dicke parameter η is 0.03. Figure 2 shows the result of the simulation in the case that the heating rate is not considered. The solid and dashed lines show the cases where $\Gamma_{\mathrm{eff}}/2\pi=1$ and 10 kHz, respectively. In the absence of heating, $\langle n\rangle_{\mathrm{SS,opt}}$ is limited to $\sim(\Gamma_{\mathrm{eff}}/\omega)^2$. In this case, the value of Γ_{eff} should be decided by balance of achievable $\langle n\rangle_{\mathrm{SS,opt}}$ and time to be able to spend it on cooling. As described below, this is not the case in the presence of appreciable heating.

In a more realistic case where heating is considered, the value of Γ_{eff} should be chosen from the appropriate range. We have simulated $\langle n\rangle_{\mathrm{SS,opt}}$ for the typical heating rates

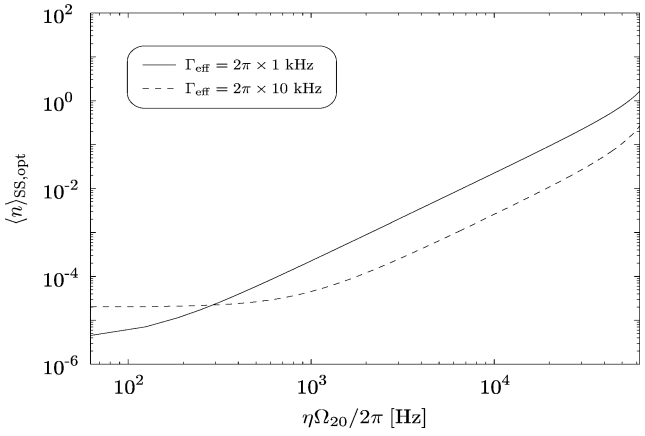

Fig. 2 Final oscillation quantum number $\langle n\rangle_{\mathrm{SS,opt}}$ as a function of $\eta\Omega_{20}$ when the heating rate is not considered. The *solid* and *dashed lines* show $\Gamma_{\mathrm{eff}}/2\pi=1$ and 10 kHz, respectively

Table 1 Parameters used for simulations

Parameter	Value
$\Gamma_{10}/2\pi$	21.5 MHz
$\Gamma_{12}/2\pi$	1.6 MHz
$\Gamma_{00}/2\pi$	5 kHz
$\Gamma_{11}/2\pi$	500 kHz
$\omega/2\pi$	2.4 MHz
θ	60°

[5–9, 16–23] reported previously. Figure 3 shows the dependence of $\langle n\rangle_{\mathrm{SS,opt}}$ for $\eta\Omega_{20}$ with R_{heat} (a) 1000, (b) 100, and (c) 10 s^{-1}. Here, the linewidth of 729 nm laser $\Gamma_{00}/2\pi$ is fixed to 5 kHz (see Table 1). The solid lines shows the optimum values for Γ_{eff} that minimize $\langle n\rangle_{\mathrm{SS,opt}}$. As shown in Fig. 3, $\langle n\rangle_{\mathrm{SS,opt}}$ is minimized when Γ_{eff} is approximately $2\pi \times 15$ kHz, and the value of the optimum Γ_{eff} is found to be rather insensitive to the heating rate. The dashed or dotted curves show simulated results for different Γ_{eff} that gives by one order higher minimum values for $\langle n\rangle_{\mathrm{SS,opt}}$. Figure 3 shows that $\langle n\rangle_{\mathrm{SS,opt}}$ increases by only one order higher minimum values even if we change the value of Γ_{eff} between several ten Hz and several hundred kHz.

It is found that the value of the optimum Γ_{eff} depends on the linewidth of the 729 nm laser Γ_{00}. The relation between the optimum Γ_{eff} and Γ_{00} is shown in Fig. 4. As shown in Fig. 4, the optimum Γ_{eff} is nearly proportional to Γ_{00}, with the proportionality coefficient $\Gamma_{\mathrm{eff}}/\Gamma_{00}$ of about 3. The heating rate assumed for the result in Fig. 4 is 100 s^{-1}, however, the proportionality coefficient is found to hardly depend on R_{heat}. On the other hand, the optimum Rabi frequency of 729 nm beam $\eta\Omega_{20}$ that minimizes $\langle n\rangle_{\mathrm{SS,opt}}$ depends on R_{heat}. Figure 5 shows the relation between the optimum $\eta\Omega_{20}$ and R_{heat}. As shown in Fig. 5, the optimum $\eta\Omega_{20}$ depends almost linearly on R_{heat}. $\eta\Omega_{20}$ also depends on Γ_{00}; therefore, we should increase the value of $\eta\Omega_{20}$ if the linewidth of the laser used for sideband cooling is relatively large.

We try to explain the above mechanism qualitatively. We numerically found that the optimum value of $\langle n\rangle_{\mathrm{SS}}$ is determined by a balance of at least five contributing factors in case that the heating rate and the laser linewidth are considered. Among these factors, two factors depend on R_{heat}. Even if R_{heat} changes, however, the contributions to the optimum Γ_{eff} by the two factors are canceled each other. Therefore, the optimum Γ_{eff} is hardly affected by the change of R_{heat}.

On the other hand, if Γ_{00} becomes higher, an excitation rate on the off-resonance transition increases while that on the resonance transition decreases. It causes a decrease of the cooling rate W, and the effect of heating by R_{heat} becomes remarkable, especially in the range of $\Gamma_{\mathrm{eff}} \ll \Gamma_{00}$. In addition, an excitation rate on the carrier transition increases

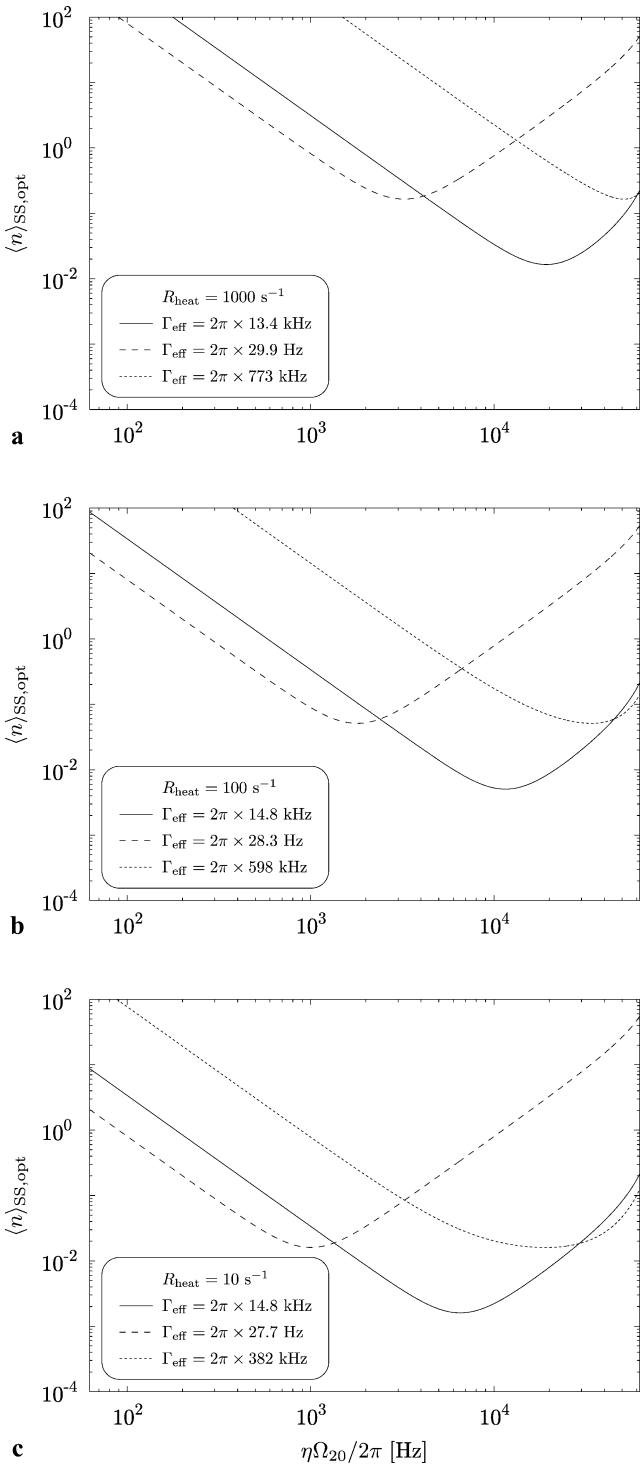

Fig. 3 Final oscillation quantum number $\langle n\rangle_{\mathrm{SS,opt}}$ as a function of $\eta\Omega_{20}$ with the inclusion of typical heating rates. Figures show the results for R_{heat}: (**a**) 1000, (**b**) 100, and (**c**) 10 s^{-1}. The *solid lines* show the optimum Γ_{eff} to minimize $\langle n\rangle_{\mathrm{SS,opt}}$. The *dashed* and *dotted lines* show the values of Γ_{eff} that give by one order higher minimum values for $\langle n\rangle_{\mathrm{SS,opt}}$

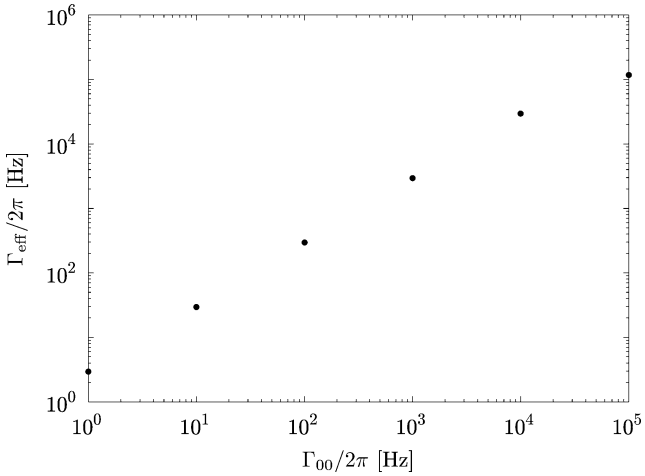

Fig. 4 Relation between the optimum $\Gamma_{\rm eff}$ and Γ_{00}. The optimum $\Gamma_{\rm eff}$ is nearly proportional to Γ_{00}. The proportionality coefficient hardly depends on $R_{\rm heat}$

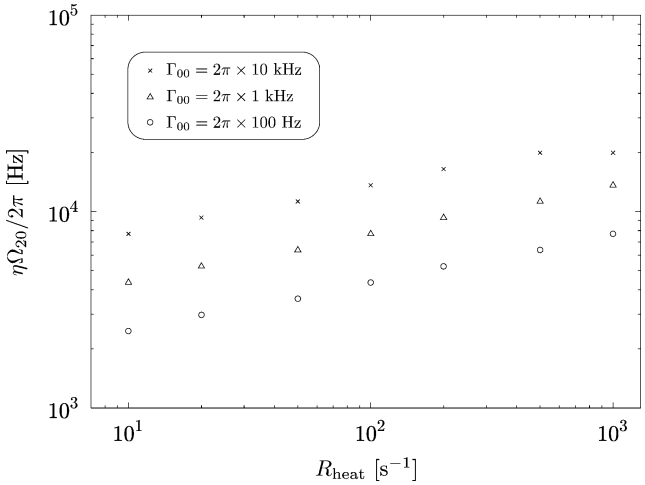

Fig. 5 Relation between the optimum $\eta\Omega_{20}$ and $R_{\rm heat}$ for various Γ_{00}. The *circle*, *triangle*, and *cross marks* belong to $\Gamma_{00}/2\pi = 0.1$, 1, 10 kHz, respectively. The optimum $\eta\Omega_{20}$ depends almost linearly on $R_{\rm heat}$

in the range of $\Gamma_{\rm eff} \ll \Gamma_{00}$. It may increase the population on the upper level, and consequently causes heating by stimulated emission. As a result, the $\langle n \rangle_{\rm SS}$ is minimized when the optimum $\Gamma_{\rm eff}$ shifts toward a higher direction by a balance of other contributing factors.We found that the optimum $\Gamma_{\rm eff}$ is almost proportional to Γ_{00} in the range of $\Gamma_{00} \ll \omega$. This proportional relation is violated when Γ_{00} approaches ω.

4 Procedure for the experimental verification of the numerical analysis

For the verification of the numerical analysis described in Sect. 3, we perform sideband cooling of $^{40}Ca^{+}$ and measure achieved average oscillation quantum numbers. Experimental procedure is shown as follows.

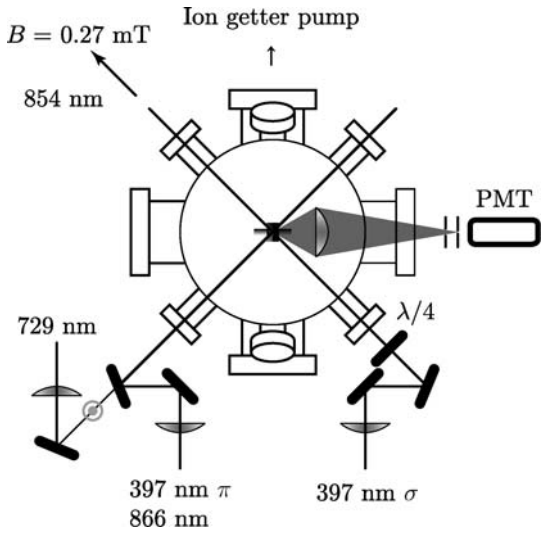

Fig. 6 A schematic of the experimental setup

4.1 Experimental setup

In the experiment, a spherical Paul trap consisting of a ring and two end-cap electrodes is used. The ring has an inner radius of $r_0 = 0.6$ mm, and the distance between the center of trap and one of the end-caps is $z_0 = 0.42$ mm. The material of these electrodes is stainless SUS304. The trap is mounted in a vacuum chamber, whose background pressure is kept at 3×10^{-8} Pa. An RF voltage of $V_{\rm RF} = 200$ V at $\Omega_{\rm RF} = 2\pi \times 20$ MHz and a DC voltage of $V_{\rm DC} = 5$ V are applied between the ring and end-cap electrodes. The applied field produces a secular potential with radial and axial frequencies of $(\omega_{\rm rad}, \omega_{\rm ax}) = 2\pi \times (1.7, 2.4)$ MHz, respectively.

A schematic of the experimental setup is shown in Fig. 6. The detail of the setup is described in [24]. A single $^{40}Ca^{+}$ ion is loaded by the electron-impact ionization method. The loaded ion is Doppler cooled by applying 397 and 866 nm beams. Fluorescence, on the $S_{1/2}$–$P_{1/2}$ transition, from the single $^{40}Ca^{+}$ ion is detected by a photomultiplier tube (PMT) to be used for the internal state determination. Fluorescence photons of 10000 counts/s are typically collected from the single ion. A titanium sapphire (Ti:Sa) laser is used for the excitation of the $|0\rangle$–$|2\rangle$ transition. As a stable frequency reference, a temperature-controlled high finesse cavity made of ultra low expansion (ULE) glass is prepared. The ULE cavity is mounted in a vacuum chamber. The 729 nm laser is locked to the ULE cavity using the Pound–Drever method [25]. The linewidth of the 729 nm laser Γ_{00} is estimated to be $2\pi \times 5$ kHz from the fluctuation of the Pound–Drever error signal. Alternatively, we

observed the carrier on the $S_{1/2}$–$D_{5/2}$ transition by applying this laser to the ion, and obtained a linewidth of less than 10 kHz. Though this linewidth includes the contribution of magnetic field fluctuations, we deduce the laser has a linewidth Γ_{00} of around $2\pi \times 5$ kHz.

4.2 Sideband cooling

Motional ground state cooling is achieved by using a laser pulse sequence, consists of five periods: *Doppler cooling*, *optical pumping*, *sideband cooling*, *shelving*, and *observation* periods. (i) Doppler cooling period: the trapped ion is Doppler cooled by the linearly polarized 397 nm (397 nm π) beam for 2 ms. The average vibrational quantum number of the Doppler-cooled ion is typically $\langle n \rangle < 5$ for the axial direction (the details are shown in [24]). (ii) Optical pumping period: the ion is prepared in the $|0\rangle$ level by applying the circularly polarized 397 nm (397 nm σ) beam for 250 μs along the direction orthogonal to the 397 nm π beam. A magnetic field of 0.27 mT is applied along the direction parallel to the 397 nm σ beam. (iii) Sideband cooling period: the ion is sideband-cooled to near the motional ground state by applying the 854 nm beam and 729 nm beam tuned resonance to the first red sideband. (iv) Shelving period: the 729 nm beam tuned resonance to the transition is applied to the ion for 1 ms. (v) Observation period: fluorescence from the ion is collected by exciting the Doppler-cooling transition for 7 ms. Thus, we can determine whether the transition to the $|2\rangle$ level has occurred or not. If the trapped ion is shelved to the $|2\rangle$ level, only few background photons are detected. The 866 nm beam is continuously applied to the ion throughout the sequence. At the end of the sideband cooling, the ion is prepared in $|0\rangle$ level by applying the 397 nm σ and 854 nm beams for 250 μs. The duration for the sideband cooling period is systematically varied, and the dynamics of the cooling process is studied as is described later.

The sequence (i)–(v) is repeated typically 100 times per each data point. The 729 nm shelving beam is scanned across the axial secular frequency of $\omega_{\mathrm{ax}}/2\pi = 2.4$ MHz, and excitation probabilities are evaluated for the red/blue sideband. The average oscillation quantum number $\langle n \rangle$ of the sideband cooled ion is estimated from the equation

$$\frac{P_{\mathrm{red}}}{P_{\mathrm{blue}}} = \frac{\langle n \rangle}{\langle n \rangle + 1}, \tag{16}$$

where $P_{\mathrm{red/blue}}$ is the excitation probability for the red/blue sideband.

5 Experimental results

We first describe the experimental parameters used for the sideband cooling experiment. The intensity of the 729 nm beam is 85 W/cm^2 in the trap position, which corresponds to the Rabi frequency of $\Omega_{20} = 2\pi \times 100$ kHz. The Rabi frequency Ω_{20} is measured by observation of the Rabi oscillation between the $|0\rangle$ and $|2\rangle$ levels. The intensity of the 854 nm beam is adjusted to 4.2 mW/cm^2, corresponding to the Rabi frequency $\Omega_{12} = 2\pi \times 2.3$ MHz. Alternatively, Ω_{12} is estimated from a light shift of the $|2\rangle$ level due to the 854 nm beam. The detuning of 854 nm laser is set to $\delta_{12} = 2\pi \times (-300)$ MHz. These parameters correspond to $\Gamma_{\mathrm{eff}} = 2\pi \times 315$ Hz. The Lamb–Dicke parameter η is 0.03, and $\eta\Omega_{20}$ is fixed to $2\pi \times 3$ kHz in the present experiment.

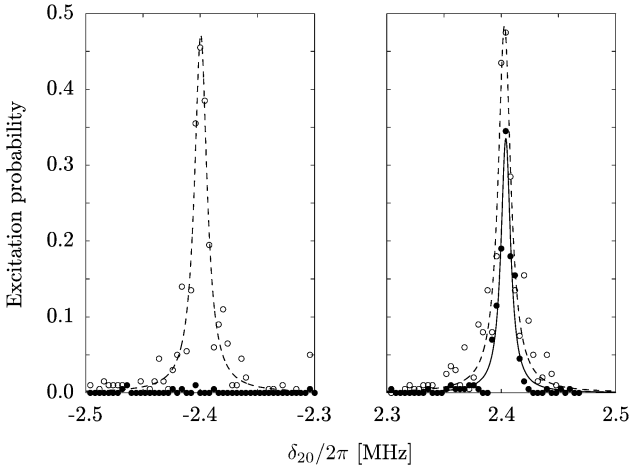

Fig. 7 Result of sideband cooling experiment. The excitation probabilities are shown for the axial *red* (*left*) and *blue* (*right*) sidebands. The *white* or *black point* shows the result for before or after sideband cooling. The achieved $\langle n \rangle$ after sideband cooling is estimated to 0.02

The result of the experiment is shown in Fig. 7. The figure of the left/right column shows the excitation probability for the axial red/blue sideband. The white and black points show the transition spectra for before and after sideband cooling, respectively. Here sideband cooling is performed for 20 ms. The achieved $\langle n \rangle$ is approximately 0.02.

The duration for the sideband cooling is systematically lengthened, and the dependence of $\langle n(t) \rangle$ on the cooling time is studied. Here the experiments are performed under two situations, referred to as Result I or II; Result I was measured in the condition where R_{heat} seemed to be relatively low value. On the other hand, Result II was measured in the condition almost same as Result I, but three months later from the measurement of Result I. Since many other experiments had been performed on the same trap during the intervening three months, the surface of the trap might have been got polluted. As pointed out in [20], this pollution of the trap surface might have caused the increase of the heating rate.

Result I and II are shown in Fig. 8. The circle symbols indicate Result I. The curve is the fit to the data set using (10). From the fit, we estimate $\langle n(0) \rangle = 4.3$, $R_{\mathrm{heat}} = 5$ s^{-1}, and $W = 420$ s^{-1}. Here it is assumed that A_+ is approximately

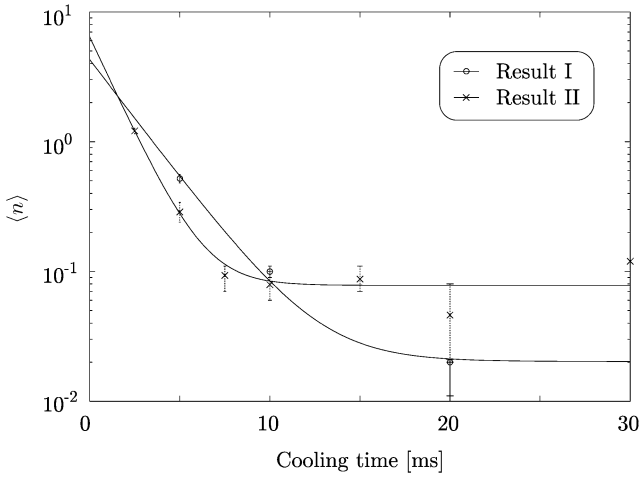

Fig. 8 $\langle n \rangle$ versus durations of sideband cooling. The *circle* or *cross symbols* show Result I or II. Curves are fitted to both data sets using (10), which evaluate the values of parameters $\langle n(0) \rangle$, R_{heat}, and W

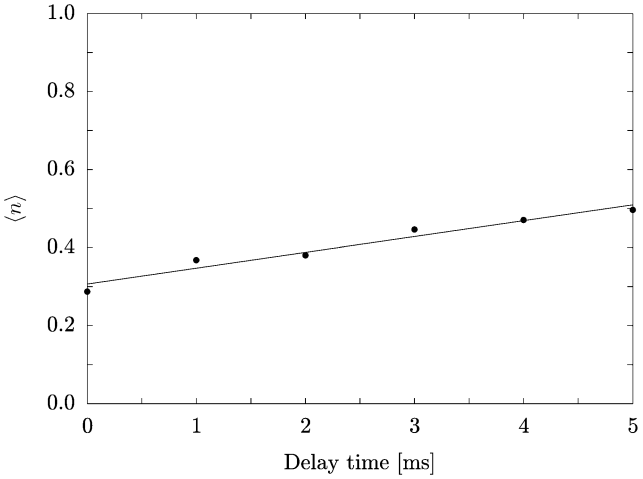

Fig. 9 The axial $\langle n \rangle$ when delay times are inserted. The *line* fitted to the data set evaluates $R_{\text{heat}} = 40.5\ \text{s}^{-1}$

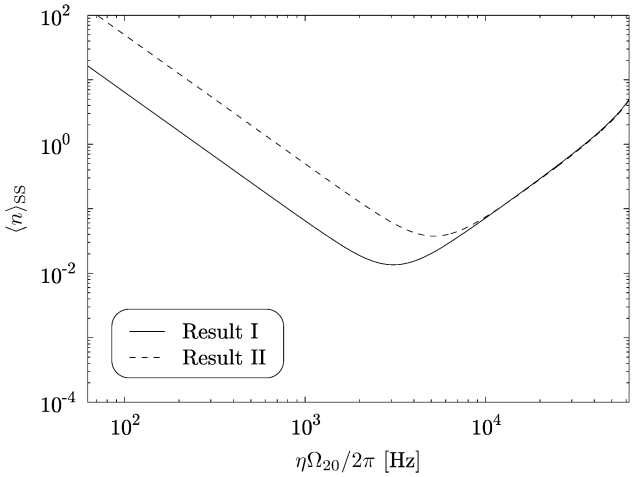

Fig. 10 Simulated $\langle n \rangle_{\text{SS}}$ for the present experimental parameters. The *solid* and *dashed lines* indicate the results for $R_{\text{heat}} = 5\ \text{s}^{-1}$ (Result I) and $40\ \text{s}^{-1}$ (Result II), respectively. The achieved $\langle n \rangle$ are approximately 0.01 and 0.06 at $\eta\Omega_{20} = 2\pi \times 3$ kHz for Results I and II, respectively

$10\ \text{s}^{-1}$ from (5) and experimental parameters. We could not estimate confidence intervals of the fitting parameters for Result I since the number of the fitting parameters is equal to that of the data points. The cross symbols indicate Result II. The fitted curve evaluates $\langle n(0) \rangle = 6.4 \pm 1.1$, $R_{\text{heat}} = 43 \pm 15\ \text{s}^{-1}$, and $W = 690 \pm 71\ \text{s}^{-1}$. From (11), the value of W is supposed to reach approximately 5000 in the present experimental parameters, that means $\langle n \rangle$ reaches $\langle n \rangle_{\text{SS}}$ in a few ms. However, W is sensitive to the drift of the laser frequency. In our case, there is 10 kHz drift in the 729 nm laser frequency during the experiment. This may reduce W to near one-tenth.

R_{heat} is directly measured for the Result II. The ion is sideband cooled for 5 ms, and delay times are inserted for a few ms. The resulting $\langle n \rangle$ for delay times is shown in Fig. 9. A straight line is fitted to the data set, and estimated $R_{\text{heat}} = 40.5 \pm 5.0\ \text{s}^{-1}$. We could not directly measure the heating rate about Result I. However, we consider its value is $5\ \text{s}^{-1}$ since the heating rate from the direct measurement for Result II is comparable to the value measured through the cooling dynamics.

The spectral density of the electric field fluctuations is deduced from the present R_{heat}. For an ion trapped by a combination of static fields and inhomogeneous rf fields, the heating rate is generalized to

$$\frac{d}{dt}\langle n \rangle = \frac{e^2}{4m\hbar\omega} S_E(\omega), \tag{17}$$

where e is the charge of the trapped ion, and S_E has an unit of $(\text{V/m})^2\ \text{Hz}^{-1}$ [26]. From (17), $S_E(\omega) = 6.6 \times 10^{-13}$ $(\text{V/m})^2\text{Hz}^{-1}$ at $\omega = 2\pi \times 2.4$ MHz and $d\langle n \rangle/dt = 40\ \text{s}^{-1}$. The distance between the ion and the closest electrode is $z_0 = 0.42$ mm in the present experiment. In this case, the value of S_E is positioned at the center of the gray band of Fig. 6 shown in [23].

The achieved $\langle n \rangle_{\text{SS}}$ can be simulated for the present experimental condition. Figure 10 shows the results when $\Gamma_{\text{eff}} = 2\pi \times 315$ Hz, where $\Omega_{12} = 2\pi \times 2.3$ MHz and $\delta_{12} = 2\pi \times (-300)$ MHz. The solid or dashed line indicates Result I ($R_{\text{heat}} = 5\ \text{s}^{-1}$) or II ($R_{\text{heat}} = 40\ \text{s}^{-1}$). Here, it seems that the 729 nm laser used in the present experiment has frequency drift of about 10 kHz during the typical measurement time. To consider the effect of this drift, we assume that δ_{20} is effectively shifted by $2\pi \times (+10)$ kHz. As shown in Fig. 10, $\langle n \rangle$ at $\eta\Omega_{20} = 2\pi \times 3$ kHz are obtained to be approximately 0.01 and 0.06 for Results I and II, respectively. These values are close to the values derived from the experiment, 0.02 and 0.08, respectively.

Finally, this experiment was performed with $\Gamma_{\text{eff}} = 2\pi \times$ 315 Hz, and it is not a *real* optimum value. However, the

value seems to be optimum in our present experimental setup, and it is consistent with the result of the numerical analysis. In addition, the resulting $\langle n \rangle_{SS}$ in the present case, is not greatly different from ideally minimized $\langle n \rangle_{SS}$. We are sure that we can achieve the real optimum value if we can improve the performance of the experimental setup.

6 Conclusion

As a representative of three-level ions, optimum conditions for sideband cooling of $^{40}Ca^{+}$ are numerically analyzed. From the analysis, it is found that the optimum parameters for sideband cooling to the motional ground state depend on the heating rate and the laser linewidth. Using parameters expected from the analysis, a single $^{40}Ca^{+}$ is sideband-cooled. The achieved average oscillation quantum numbers and the optimum experimental parameters are close to the values deduced from the analysis.

References

1. J.I. Cirac, P. Zoller, Phys. Rev. Lett. **74**, 4091 (1995)
2. J.I. Cirac, R. Blatt, P. Zoller, Phys. Rev. A **46**, 2668 (1992)
3. I. Marzoli, J.I. Cirac, R. Blatt, P. Zoller, Phys. Rev. A **49**, 2771 (1994)
4. D. Reiß, A. Lindner, R. Blatt, Phys. Rev. A **54**, 5133 (1996)
5. F. Diedrich, J.C. Bergquist, W.M. Itano, D.J. Wineland, Phys. Rev. Lett. **62**, 403 (1989)
6. C. Monroe, D.M. Meekhof, B.E. King, S.R. Jefferts, W.M. Itano, D.J. Wineland, Phys. Rev. Lett. **75**, 4011 (1995)
7. Ch. Roos, Th. Zeiger, H. Rohde, H.C. Nägerl, J. Eschner, D. Leibfried, F. Schmidt-Kaler, R. Blatt, Phys. Rev. Lett. **83**, 4713 (1999)
8. L. Deslauriers, P.C. Haljan, P.J. Lee, K.-A. Brickman, B.B. Blinov, M.J. Madsen, C. Monroe, Phys. Rev. A **70**, 043408 (2004)
9. Q.A. Turchette, D. Kielpinski, B.E. King, D. Leibfried, D.M. Meekhof, C.J. Myatt, M.A. Rowe, C.A. Sackett, C.S. Wood, W.M. Itano, C. Monroe, D.J. Wineland, Phys. Rev. A **61**, 063418 (2000)
10. D.J. Wineland, W.M. Itano, Phys. Rev. A **20**, 1521 (1979)
11. D.F.V. James, Appl. Phys. B **66**, 181 (1998)
12. A. Kreuter, C. Becher, G.P.T. Lancaster, A.B. Mundt, C. Russo, H. Häffner, C. Roos, W. Hänsel, F. Schmidt-Kaler, R. Blatt, Phys. Rev. A **71**, 032504 (2005)
13. M. Lindberg, S. Stenholm, J. Phys. B: At. Mol. Phys. **17**, 3375 (1984)
14. S. Stenholm, Rev. Mod. Phys. **58**, 699 (1986)
15. J. Javanainen, S. Stenholm, Appl. Phys. **21**, 35 (1980)
16. B.E. King, C.S. Wood, C.J. Myatt, Q.A. Turchette, D. Leibfried, W.M. Itano, C. Monroe, D.J. Wineland, Phys. Rev. Lett. **81**, 1525 (1998)
17. C. Tamm, D. Engelke, V. Bühner, Phys. Rev. A **61**, 053405 (2000)
18. H. Rohde, S.T. Gulde, C.F. Roos, P.A. Barton, D. Leibfried, J. Eschner, F. Schmidt-Kaler, R. Blatt, J. Opt. B **3**, S34 (2001)
19. M.A. Rowe, A. Ben-Kish, B. Demarco, D. Leibfried, V. Meyer, J. Beall, J. Britton, J. Hughes, W.M. Itano, B. Jelenković, C. Langer, T. Rosenband, D.J. Wineland, Quantum Inf. Comput. **2**, 257 (2002)
20. R.G. DeVoe, C. Kurtsiefer, Phys. Rev. A **65**, 063407 (2002)
21. D. Stick, W.K. Hensinger, S. Olmschenk, M.J. Madsen, K. Schwab, C. Monroe, Natl. Phys. **2**, 36 (2006)
22. L. Deslauriers, S. Olmschenk, D. Stick, W.K. Hensinger, J. Sterk, C. Monroe, Phys. Rev. Lett. **97**, 103007 (2006)
23. R.J. Epstein, S. Seidelin, D. Leibfried, J.H. Wesenberg, J.J. Bollinger, J.M. Amini, R.B. Blakestad, J. Britton, J.P. Home, W.M. Itano, J.D. Jost, E. Knill, C. Langer, R. Ozeri, N. Shiga, D.J. Wineland, Phys. Rev. A **76**, 033411 (2007)
24. H. Sawamura, K. Toyoda, S. Urabe, Jpn. J. Appl. Phys. **46**, 1713 (2007)
25. R.W.P. Drever, J.L. Hall, F.V. Kowalski, J. Hough, G.M. Ford, A.J. Munley, H. Ward, Appl. Phys. B **31**, 97 (1983)
26. R.W.P. Drever, J.L. Hall, F.V. Kowalski, J. Hough, G.M. Ford, A.J. Munley, H. Ward, Fortschr. Phys. **46**, 363 (1998)